Hindawi
Applied and Environmental Soil Science
Volume 2022, Article ID 4291699, 12 pages
https://doi.org/10.1155/2022/4291699

Research Article

Sediment Yield Modeling and Mapping of the Spatial Distribution of Soil Erosion-Prone Areas

Chala Hailu Sime and Wondmagegn Taye Abebe

Faculty of Civil and Environmental Engineering, Jimma University, Jimma 378, Ethiopia

Correspondence should be addressed to Chala Hailu Sime; chala.sime@ju.edu.et

Received 13 June 2022; Accepted 17 August 2022; Published 2 September 2022

Academic Editor: Venkatramanan Senapathi

Sediment movement is the most critical problem in Ethiopia, notably in the Ketar River watershed, which is located in the Rift Valley Basin. The Ketar River flows through rugged terrain with steep slopes and high sediment movement. The purpose of the study is to evaluate the Soil and Water Assessment Tool's (SWAT) ability to simulate sediment and to identify areas that are vulnerable to soil erosion. This will aid water resource planners in determining the appropriate corrective action. In SWAT sediment sensitivity analysis, the USLE soil erodibility factor (USLE-K) is found to be the most sensitive sediment parameter. The SWAT model sediment simulation performance is evaluated using the coefficient of determination (R^2) and Nash-Sutcliffe Efficiency (NSE). The model performance results in R^2 and NSE values of 0.69 and 0.55 for calibration and 0.73 and 0.51 for validation, respectively, using the SWAT Calibration and Uncertainty Program (SWAT-CUP). The sediment-prone area subbasins have steep slopes and were mostly covered by cultivated land. Annual sediment yield from cultivated land was approximately 1872.12 t/y, while yield for moderately cultivated grassland was 171.45 t/y. Woodland and forest land have less soil erosion rate. The subbasin highly covered by Eutric Nitisols is found in very high soil erosion-prone areas. Sediment yield from a slight slope is almost zero, whereas sediment yield from steep and very steep slopes is very high. The slope of the subbasin is an important factor in determining sediment yield, followed by land cover and soil types. The very high sediment yield rate area accounted for 39.64% of the total subbasin and it needs soil conservation planning.

1. Introduction

Soil erosion is the accelerated removal of topsoil by water, wind, or labor from the land surface [1]. The soil particles from sloping and barren fields are washed away by runoff. Large amounts of fine sediments are mobilized in the watershed as a result of rainstorms [2]. Erosion from the surface of the soil takes the form of plate erosion, rill erosion, and erosion between river banks (gully erosion). Soil water repellence can impair the infiltration of water and perhaps cause soil erosion [3]. Rainfall causes dissociation of the soil, erosion, and deposition. Plunging and discharge are the main factors that cause soil erosion and movement from the river bottom to downstream [4].

Soil erosion is one of the most serious environmental problems and is a serious threat to food safety and the world's ecology. More than 99.7% of the world's food sources are based on land, and only around 0.3% are from the oceans and other aquatic environments. Every year, roughly ten million hectares are lost because of soil erosion in the world. This causes a reduction in the amount of cropland available for food production [5].

Soil erosion is more intense in developing countries due to their poor land use and land cover management system. Africa is highly affected by soil erosion and is followed by Asia [6]. The rapid population expansion in the world, particularly in developing countries, causes an expansion of the agricultural land for food production [7]. Ethiopia's population is rapidly expanding, and livestock is being retained very densely, particularly in the Ketar watershed, which is part of the Rift Valley Basin. Forest and grassland are transformed into cultivated land upstream of the watershed. Long and steep gradients of the watershed which were turned into cultivated land without the proper

protection measures made the land surface vulnerable to soil erosion through runoff. High-intensity rainfall also leads to severe erosion and sedimentation [8, 9]. So, it is required to model sediment yield from the watershed and identify prone areas using appropriate hydrological models.

The Soil and Water Assessment Tool is the physical-based, semidistributed, and continuous-time model used to simulate the water and sediment yield in basins over extensive periods all over the world [10]. Weather data (rainfall, temperature, relative humidity, wind speed, and solar radiation) and spatial data (land use, soil texture, and Digital Elevation Model) are the main input in the SWAT. SWAT is used to simulate hydrological parameters in the watershed. It is a well-known and efficient tool that has been successfully used to simulate runoff [9, 11]. The SWAT is also used to predict maximum sediment loads [12, 13]. Multiple studies in Ethiopia show that the SWAT model performs well in sediment yield modeling [14–16]. The study by [17] found that the SWAT model performs better than other models and has a tolerable level of uncertainty. In this study, the SWAT (2012 Version) model simulated sediment yield and located the soil erosion hot spots in the Ketar River watershed, Rift Valley Basin, Ethiopia.

The sediment yield modeling in the watershed will assist many stakeholders to reduce land degradation, boost plant cover, and improve watershed productivity. For this purpose, decision-makers need to design watershed management plans for better soil and water conservation strategies that model the quantity of sediment yield from the catchments into streams, rivers, and water bodies. Reducing soil erosion and transportation is the key to sustainability in agricultural production and productivity and helps preserve food security.

2. Materials and Methods

2.1. Description of the Study Area. The Ketar River is located in Ethiopia's Rift Valley Basin. It is located between the latitudes 7.16° to 8.31° N and longitude 38.69° to 39.62° E. Topographically, the Ketar range has a strong elevation fluctuation of around 1620 meters on Lake Ziway to 4178 m on the high volcanic ridge mountains of the eastern watershed. The total watershed of the study area is about 3360 km^2 in total. Figure 1 shows a map of the study area.

2.2. Data Collection and Analysis. The spatial data (soil maps, land use/land cover) were collected from the Ministry of Water and Irrigation and Energy (MoWIE) of Ethiopia. The land use/land cover data for 2016 was used in this study. The Digital Elevation Model (DEM) was obtained from https://vertex.daac.asf.alaska.edu/. Weather data (precipitation, temperature, solar radiation, relative humidity, and wind speed) were collected from the National Meteorological Agency (NMA) of Ethiopia. The MoWIE also provided the sediment data used for calibration and validation. Weather data for 29 years (1988 to 2017) from six meteorological stations in the study area were collected. The selection of the meteorological stations is based on the availability of the data. Table 1 shows the locations of the meteorological stations.

2.2.1. Soil Data. The soil database describes the watershed's surface and top surface. The soil type used in this study was extracted from the Ethiopian soil database. The Ketar River watershed contains nine major soil types, Eutric Cambisols, Chromic Luvisols, Mollic Andosols, Vitric Andosols, Haplic Xerosols, Eutric Fluvisols, Vertic Cambisols, Eutric Nitisols, and Pellic Vertisols, as shown in Figure 2. Eutric Nitisols covered a large portion of the watershed.

Nitisols are deep, well-drained red soils with diffuse horizon boundaries and a subsurface horizon with more than 30% clay. Nitisols are predominantly located on flat to hilly land in the watershed. Nitisols are among the most productive agricultural soils along with Vertisols, Luvisols, and Planosols. Despite their low levels of available phosphorus and low base status, they are often considered to be "fertile" soils. Nitisols are deep and stable soils with good physical characteristics [18].

Chromic Luvisols are mainly characterized by a distinct textural heterogeneity within the soil profile. In these soils, clay is washed down from the surface soil to an accumulation horizon at a certain depth. Luvisols are most common in cool as well as warm temperate regions with distinct dry and wet seasons. Luvisols with good internal drainage are potentially suitable for a wide range of agricultural uses because of their moderate stage of weathering and high base saturation. Mollic Andosols, Vitric Andosols, and Haplic Xerosols are found on the watershed's low land, which is covered in grassland and shrubland. Mollic Andosols and Vitric Andosols are rich in clay, whereas Haplic Xerosols are rich in loam. Clay and loam are abundant in Eutric Cambisols. Cultivated land covers a large portion of this soil type. Pellic Vertisols are found in hilly and mountainous areas where alpine vegetation dominates the land use [19]. Figure 2 illustrates the soil types of the Ketar River watershed.

Table 2 shows the SWAT soil code, soil type, soil textures, and the percentage of the area coverage.

2.2.2. Land Use/Land Cover. There are six dominant land use and land cover types in the Ketar River watershed as shown in Table 3 and Figure 3. The large area of the watershed is covered by intensively cultivated agricultural land. It accounts for 67.22% of the total land use. The mountainous area of the watershed is covered by alpine vegetation or forest-mixed. The land downstream of the watershed is shrub land.

2.3. Slope Distribution in Ketar River Watershed. The watershed has a varied slope. Gently sloping terrain accounts for approximately 57% of the watershed. A very steep slope accounts for only 2.91% of the total area and is found on the watershed's high land, where the land use/land cover is covered by alpine vegetation. The cultivated land is heavily covered by flat to gently sloping terrain. The slope class in Ketar River watershed is shown in Table 4 and Figure 4.

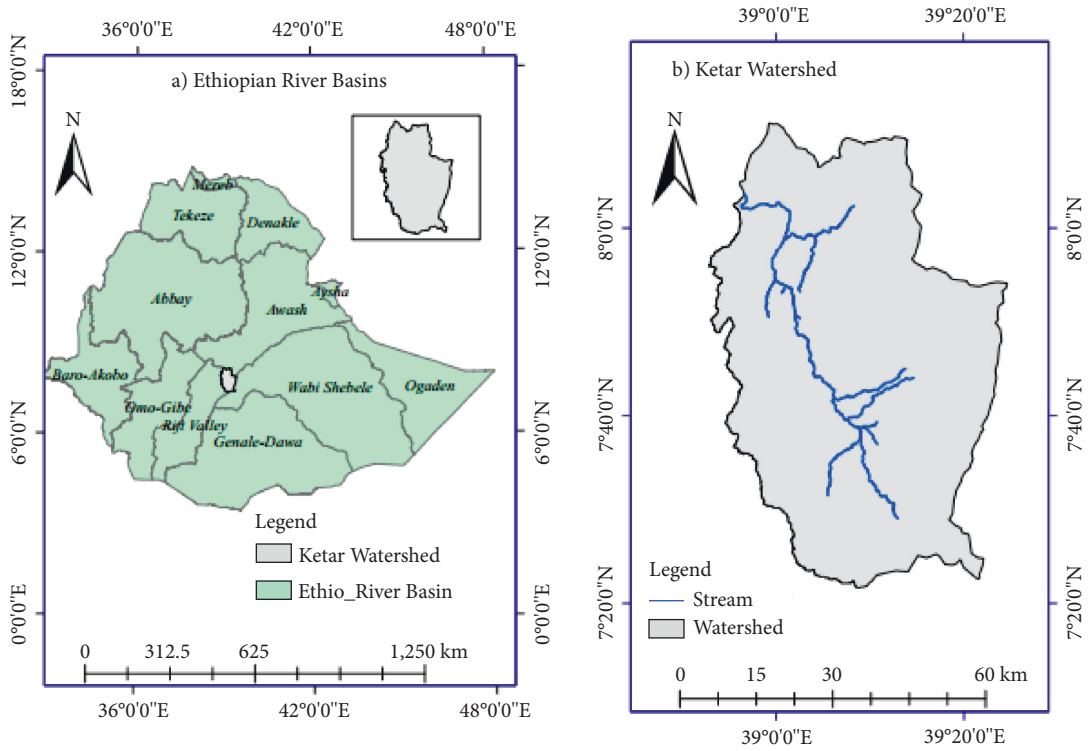

Figure 1: Map of the study area.

Table 1: Locations of the meteorological stations.

Station name	Latitude	Longitude	Altitude
Arata	7.96	39.06	1770
Kulumsa	8.01	39.16	2211
Munesa	7.53	38.98	2550
Bekoji	7.53	39.25	2850
Sagure	7.75	39.16	2480

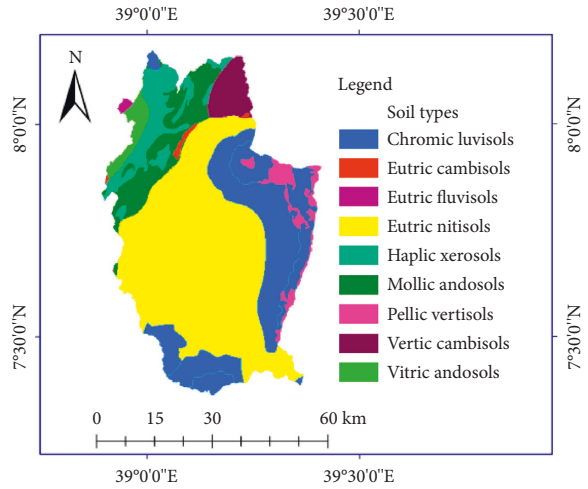

Figure 2: Soil types of the Ketar River watershed.

Table 2: Dominant soil types in the watershed with their corresponding percentage of coverage.

SWAT soil code	Soil name	Area (km^2)	Soil textures	Area coverage (%)
Be56-2-3a-456	Eutric Cambisols	13.85	Clay and loam	0.41
Nh7-2-3c-854	Chromic Luvisols	862.75	Clay and loam	25.66
Vc14-3a-261	Mollic Andosols	290.95	Clay	8.65
Vc25-3a-263	Vitric Andosols	71.03	Clay	2.11
Xh17-2a-310	Haplic Xerosols	235.89	Loam	7.02
Fo94-2ab-556	Eutric Fluvisols	9.01	Sandy clay and loam	0.27
Be64-1-2a-461	Vertic Cambisols	130.08	Sandy loam	3.87
Nd3-1565	Eutric Nitisols	1646.38	Loam	48.96
Vc40-3a-956	Pellic Vertisols	102.47	Clay	3.05

Table 3: Land use/land cover and percentage of area coverage.

Name	Description	SWAT code	Area (km^2)	Area %
Cultivation	Intensively cultivated	CORN	2260.25	67.22
Shrub land	Shrub land/mixed grassland	MIGS	124.72	3.71
Grassland	Open grassland/moderately cultivated	RNGB	564.39	16.79
State farms	Durum wheat	DWHT	15.33	0.46
Open woodland	Woodland mosaic	CRWO	18.41	0.55
Alpine vegetation	Afroalpine heath vegetation	FRST	379.33	11.28

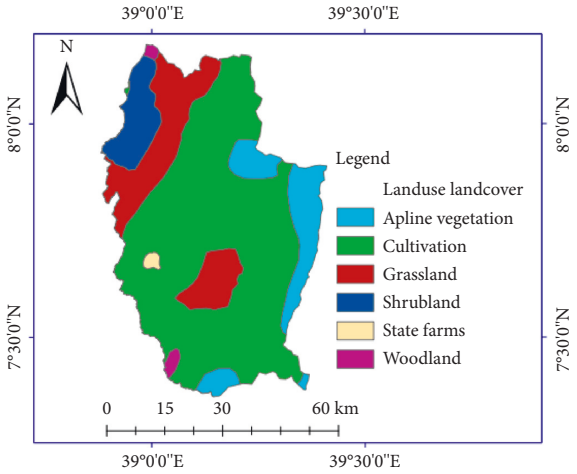

Figure 3: Ketar River watershed land use/land cover.

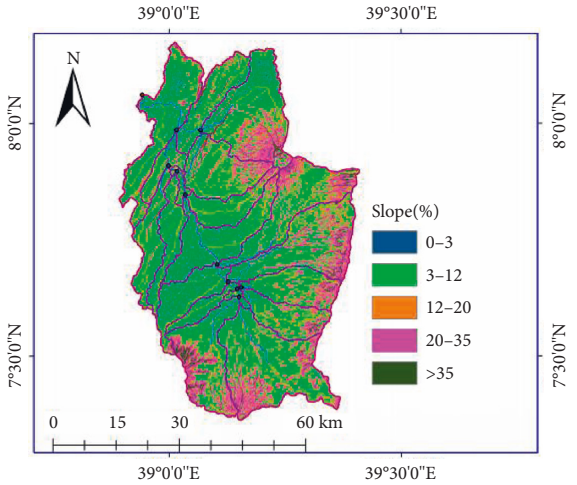

Figure 4: Slope distribution in the Ketar River watershed.

Table 4: Slope class in Ketar River watershed.

Slope class (%)	Area (km^2)	Area %	Slope
0–3	425.55	12.66	Flat
3–12	1914.02	56.92	Gently sloping
12–20	569.86	16.95	Sloping
20–35	355.09	10.56	Steep
>35	97.90	2.91	Very steep

2.4. Sediment Data. Sediment data are generated to evaluate long-term watershed sediment yields. The sediment rating curve was used as a basis for the continuous-time generation of sediments in the river. The sediment data were collected downstream of the watershed, at Abura gaging station (38°58′59″E and 8°2′32″N). The sediment rating curve is a link between the discharge and the concentration or loading of sediments [20]. A load of sediment carried by a river is generally estimated. The average sediment level or load may be shown as a result of daily, monthly, or other periods of average discharge. The discharge recorded is converted to sediment concentration or load records by the rating curve [21]. A sediment rating curve relates to the suspended sediment concentration in a river with water discharge. Commonly, the relationship is of the following form [22]:

$$\mathrm{Qs} = aQ^b, \tag{1}$$

$$\mathrm{Or\ LogQs} = \mathrm{Log}a + b\mathrm{LogQ}, \tag{2}$$

where Q is the discharge (m^3/s); Qs is sediment discharge, in tons per day; a and b are constants. The constants a and b are solved by applying the equations for a simple linear regression [22] to logarithmically transformed values of water discharge and sediment discharge as shown in the three following equations:

$$b = \sum \log Q * \log Qs - N * \frac{\overline{\log Q} * \overline{\log Qs}}{\sum (\log Q)^2 - N\overline{(\log Q)}^2}, \quad (3)$$

$$\log a = \overline{\log Qs} - b\overline{\log Q}, \quad (4)$$

$$a = \text{anti}\log\overline{(\log Qs)} - b\overline{\log Q}, \quad (5)$$

where $\overline{\log Qs}$ is the average of sediment discharge values (logarithms), $\overline{\log Q}$ is the average of water discharge values (logarithms), and N is the number of paired observations.

In this study, by applying the above equations ((1)–(5)) to the recorded sediment concentration and corresponding streamflow recorded at Abura station, sediment discharge developed as shown in the following equation:

$$Qs = 8.9Q^{1.77}, \quad (6)$$

where Qs is sediment discharge in tons per day; Q is water discharge in cubic meters per second; and $a = 8.9$ and $b = 1.77$.

Regression equations for sediment concentration versus water discharge can be put into a similar form as those for sediment discharge to compute sediment discharge from sediment concentration as shown in equation (7):

$$Qs = 0.0864C * Q, \quad (7)$$

The relation between sediment concentration and water discharge becomes as shown in the four following equations:

$$0.0864CQ = aQ^b, \quad (8)$$

where

$$C = a'Q^{b'}, \quad (9)$$

$$a' = \frac{a}{0.0864}, \quad (10)$$

$$b' = b - 1. \quad (11)$$

C is sediment concentration, in milligrams per liter, and 0.0864 is a conversion factor.

Following the calculation of the sediment load, the relationship between the continuous (daily time step) measured flow in m^3/s and the measured sediment load (mg/l) was established and is as shown in the following equation:

$$C = 103 * Q^{0.77}. \quad (12)$$

2.5. Description of the SWAT Model. The SWAT model is a basin model, created for easy use with the input data provided. The SWAT model is a fluvial basin model and was initially created to represent long-term runoff and nutrient losses from rural watersheds [23]. It was created to model the hydrological conditions of an area where agricultural land dominates land use and land cover. The model is applicable because agricultural land dominates the Ketar River watershed as well. SWAT-CUP can also be used to calibrate the model's applicability [24]. The model, which is semiphysically based, divides the watershed into numerous subwatersheds, each of which is further divided into Hydrologic Response Units (HRUs) based on soil, LULC, and slope. This allows the simulation of a high level of spatial detail. Equation (13) illustrates the water balance equation used to determine the hydrological components of the watershed [24]:

$$SW_t = SW_0 + \sum_{i=1}^{t}\left(R_{day} - Q_{surf} - Ea - w_{seep} - Q_{gw}\right), \quad (13)$$

where SW_t is the final soil water content (mm H_2O), SW_0 is the initial soil water content in day i (mm H_2O), t is the time (days), R_{day} is the amount of precipitation in day i (mm H_2O), Q_{surf} is the amount of SurfQ in day i (mm H_2O), Ea is the amount of ET in day i (mm H_2O), W_{seep} is the amount of percolation in day i (mm H_2O), and Q_{gw} is the amount of return flow in day i (mm H_2O).

The Soil Conservation Service (SCS) curve number (CN) [24] given in equation (14) and daily rainfall data are used by the SWAT model to predict surface runoff and peak runoff rates for each HRU. HRU denotes the tiniest area, which is made up of LULC, soil type, and slope.

$$Q_{surf} = \frac{\left(R_{day} - I_a\right)^2}{\left(R_{day} - I_a + S\right)}, \quad (14)$$

where Q_{surf} is the accumulated runoff or rainfall excess (mm), R_{day} is the rainfall depth for the day (mm), I_a is the initial abstraction which includes surface storage, interception, and infiltration before runoff (mm H_2O), and S is the retention parameter (mm H_2O).

2.5.1. Sediment Component of SWAT. The Modified Universal Soil Loss Equation (MUSLE) was developed by Wischmeier and Smith in a modified version of the Universal Soil Loss Equation (USLE, in Spanish) [24]. The modified universal equation for soil loss is as follows:

$$Sed = 118 * \left(Q_{Surf} * Q_{Peak} * A_{hru}\right)^{0.56} * K_{USLE} * C_{USLE} * P_{USLE} * L_{SUSLE} * CFRG, \quad (15)$$

where Sed is the sediment yield on a given day in metric tons, Q_{Surf} is the surface runoff from the watershed in mm/ha, Q_{peak} is the peak runoff rate in cubic meters per second, A_{hru} is the area of HRU, K_{USLE} is the USLE soil erodibility factor, C_{USLE} is the USLE land cover and management factor, P_{USLE} is the USLE support practice factor, L_{SUSLE} is the USLE topographic factor, and CFRG is the coarse fragment factor.

2.6. SWAT Model Setup. The size of subbasins is carefully defined by determining the threshold area or minimum drainage area needed to originate the streams [25]. The threshold area defines the minimum drainage area necessary to produce a stream source. By selecting a threshold area of 11000 ha, the entire watershed was delineated into 21 subbasins.

Hydrological Response Units (HRUs) are parts of a subwatershed with unique information about a subbasin in the watershed. They are generated from the soil map, land use, and slope. All these physical parameters were superimposed for HRU definition after the reclassification of land, soil, and slope in the SWAT database [24]. In the HRU definition, 5–10% is often employed for avoiding small HRUs, reducing the overall HRUs, as well as improving the model's computational effectiveness [26, 27]. All geographical information in the watershed will be maintained by defining a threshold level for land use, soil, and slopes, because no land use, soil, or slope will be removed from the HRU distributors. In this study, multiple HRUs were used, including all types of land use and soil type and a 5% slope threshold. The SWAT write input table was used to insert weather data, and the watershed simulation component was completed using the GIS (version 10.4.1) with the SWAT 2012 model interface. Finally, after simulation, SWAT-CUP is used to analyze sensitivity as well as for calibration and validation checks. It is used to simplify the calibration procedure, provide a faster method of performing time-consuming measuring operations, and standardize calibration steps [28].

The SWAT-CUP can be calibrated and analyzed using the SUFI-2, Particle Swarm Optimization (PSO), GLUE, Parameter Solution (ParaSol), and Markov Chain Monte Carlo (MCMC) methods [28]. For this study, SUFI-2 was used, which has the advantage of combining optimization with an examination of invertedness and can handle multiple parameters. In addition, the technique is very efficient in the number of function calls and is straightforward to use [29].

2.7. Model Calibration and Validation. Model calibration is an attempt to better parameterize a pattern to a particular number of local conditions to reduce prediction uncertainty. Model calibration is carried out with care by comparing the model predictions (output) with the observed data for a specific set of assumed terms for the models' input parameters (within their respective uncertainty areas) [30]. During calibration, the parameter values are modified with the replacement, addition, or multiplication of the original values by the designed interface by altering one or two parameters at a time within the permissible scope. In a given parameter bound, the successful parameter value was the one with the lowest relative error.

In a given site-specific model, model validation means that one model can provide adequate predictions. This entails using the calibrated model without changing the specified parameter values when simulating the response over a period other than calibration [31].

2.8. Model Performance Criteria. The model's systematic and dynamic behavior can be seen by displaying simulated and observed data on the same coordinate system, and the modeler can determine whether the model is overpredicted or underpredicted. However, mathematical metrics of model performance were required to objectively evaluate the model. During the calibration and validation periods of this study, two methods were utilized to measure the model's goodness of fit. These are the Nash-Sutcliffe efficiency (NSE) coefficient and the coefficient of determination (R^2).

2.8.1. The Coefficient of Determination (R^2). R^2 is used to describe the percentage of variance in computed model data and varies between 0 and 1, where the value near 1.0 shows good model performance (good correlation) and the value close to 0.0 indicates bad model performance (poor correlation) [32].

2.8.2. Nash-Sutcliffe Efficiency (NSE) Coefficient. The NSE is used to evaluate the hydrological models' prediction capacity. NSE is a number that ranges from zero to one. According to Masih et al. [32], the general performance of the NSE in SWAT, which is >0.65, is very good; the NSE between 0.5 and 0.65 is adequate; the NSE >0.5 is satisfactory; and the NSE <0.5 is unsatisfactory for both accuracy assessments. The NSE and R^2 [33] are measured on daily or monthly time scales using the following general equations, respectively:

$$\mathrm{NSE} = 1 - \frac{\sum (Qobs - Qsim)^2}{\sum (Qobs - \overline{Qobs})^2}, \tag{16}$$

$$R^2 = \frac{\left(\sum (Qobs - \overline{Qobs}) * (Qobs - \overline{Qsim})\right)^2}{\sum (Qobs - \overline{Qobs})^2 * \sum (Qobs - \overline{Qsim})^2}, \tag{17}$$

where Qobs and Qsim refer to the observed and simulated data, respectively. $\overline{Qobs}$ and $\overline{Qsim}$ refer to the mean of the observed and simulated data, respectively.

3. Results and Discussion

3.1. Sediment Sensitivity Analysis. Eight of the most sensitive factors were shown to be more sensitive than others during the sediment simulation, although with varying sensitivity ranks. SPCON (linear factor for channel sediment routing), CH-COV2 (channel cover factor), SPEXP (exponential factor for channel sediment routing), USLE soil erodibility factor (USLE-K), USLE equation support practice factor (USLE-P), and HRU-SLP (average slope steepness) were chosen. The most sensitive parameter in the sediment simulation was determined to be the USLE soil erodibility factor (USLE-K).

3.1.1. Calibration. The model has been averaged monthly and validated. The model was calibrated using sediment measurements that were developed between 1992 and 1998. During the calibration of the models, they iteratively varied within the permissible limits until a sufficient agreement was reached between the sediment produced and the simulated sediment, and, eventually, good model suitability for the calibration of the R^2 value of 0.69 was acquired. The NSE of 0.55 further shows that the model performance was good during calibration. Figure 5 indicates the observed sediment versus simulated sediment at Abura gauging station

Statistical analysis of model performance during calibration using a regression plot also indicates a good relationship between simulated and observed sediment concentration. Figure 6 indicates the observed versus simulated sediment.

3.1.2. Validation. Validation follows the same procedures as calibration, and measured values are compared to determine whether the objective function is fulfilled. Measured watershed data sets, on the other hand, should be kept separate from data used for model calibration, and no model changes should be made during the validation process. For validation of the sediment, sediment data from the sediment rate curve was used for 5 years (1999 to 2003). The R^2 and NSE validation results were 0.73 and 0.51, respectively. The obtained R^2 value of 0.73 indicates that the model fits quite well. Besides, the objective function NSE of 0.51 indicates that the model performance was satisfactory. The model overestimates sediment concentration in some months, such as July and August. Again, the model simulated lower sediment values in January and December. Sediment observation and validation are depicted in Figure 7.

Statistical performance study utilizing regression plots also demonstrates an excellent link between the simulated and observed sediment concentration. Figure 8 indicates the observed versus simulated sediment scatter plot.

The model slightly overestimates sediment during both sediment validation and calibration. Table 5 shows the average developed and simulated sediment during calibration and validation.

3.2. Sediment Yield Hotspot Area Classification. Sediment output varies greatly from location to location. In some cases, even a small fraction of the landscape unit can contribute a disproportionate percentage of total sediment output. Sediment yield and soil erosion are due to the combined effects of land use, soil type, slope, weather, and runoff conditions.

The soil loss rate is highly related to soil type, land use, slope gradient, and runoff. The combination of these factors is responsible for determining the soil erosion severity level in the watershed. The SWAT model generates the sediment yield from each subbasin and the average annual soil loss per HRU. The sediment yield hotspot classifications are based on the characteristics of the watershed. Different researchers classify land use/land cover in different ways. In the Geleda watershed, soil loss severity is classified as low (0–11), moderate (11–18), high (18–30), very high (30–50), and severe (50–237) in tons per hectare per year [34]. According to [35], there are four types of soil loss in tons per hectare per year: very slight (0–4), slight (5–9.99), moderate (10–24.99), and severe (25–44.99). Soil erosion in the Wondo Genet watershed is classified as low (0–5), moderate (5–11), high (11–20), very high (20–30), severe (45–60), and very severe (>60) in tons per hectare per year [36]. Therefore, there are no distinct intervals between soil severity classes. In this study, the severity of soil loss rate was classified into six categories: slight, moderate, high, very high, severe, and very severe, based on different studies [34, 37–39]. Based on these classifications, the Ketar River watershed soil erosion class was discovered to have soil erosion severity levels ranging from slight to very high. Table 6 describes the class assigned for the degree of severity.

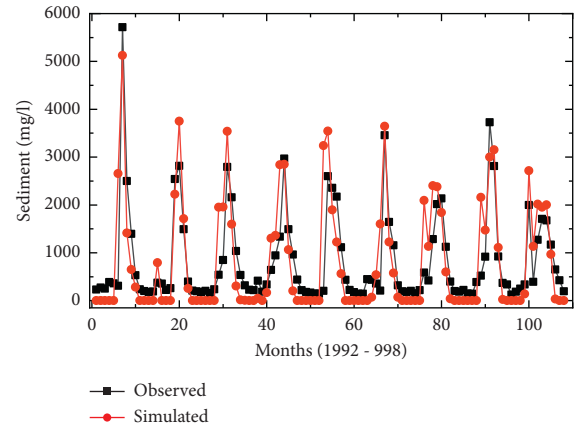

Figure 5: Observed sediment versus simulated sediment at Abura gauging station.

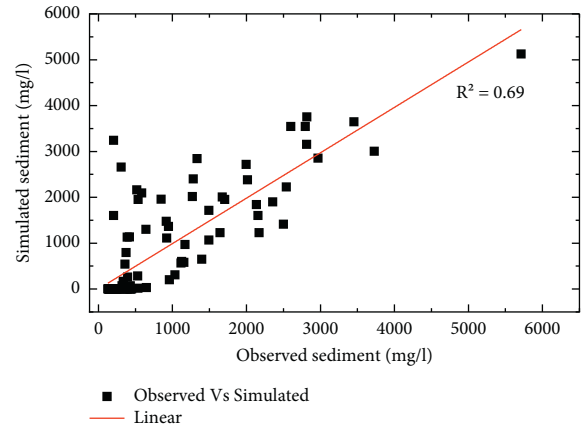

Figure 6: Observed versus simulated sediment.

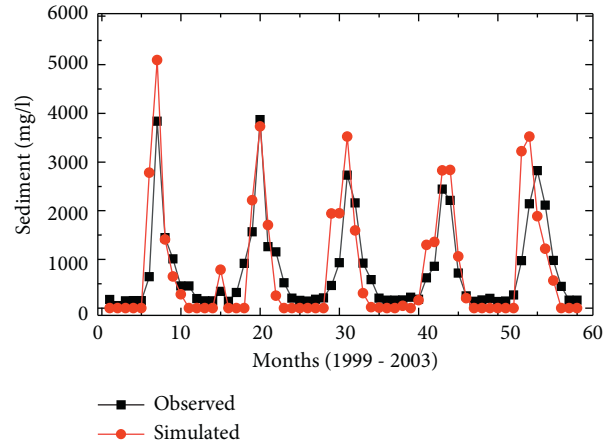

Figure 7: Observed and validated sediment.

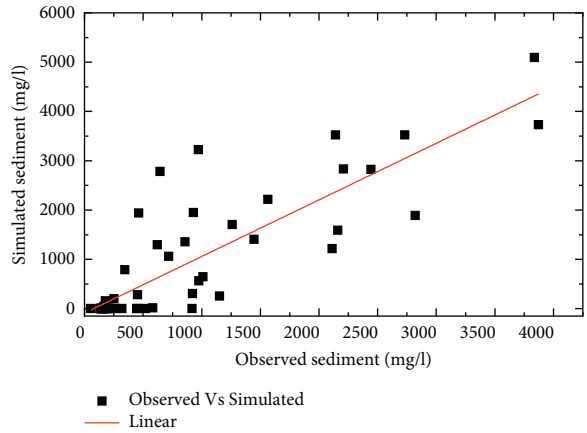

Figure 8: Observed versus simulated sediment scatter plot.

Table 5: Average observe and simulated sediment during calibration and validation.

Hydrological parameters	Observed average sediment (mg/l)	Simulated average sediment (mg/l)
Sediment calibration	828.2	820.97
Sediment validation	779.783	807.117

Table 6: Class assigned for degree of severity.

Range of sediment yield (t/ha/year)	Zone
0–4	Slight
4–8	Moderate
8–16	High
16–32	Very high
32–64	Severe
>64	Very severe

3.3. Average Annual Sediment Yield in Hotspot Subbasins. Identifying the sediment yield at the subbasin level was used to prioritize subbasins for sediment reduction management. It is also used to raise awareness about the state of the watershed in terms of soil erosion. A large area of the Ketar River watershed is found to have a high soil erosion rate. Only two subbasins are found to have a moderate soil erosion rate: subbasins 3 and 16. The very high sediment yield severity class accounts for 39.64% of the total area, accounting for approximately 1322.65 km^2. The highest simulated annual average sediment yield was found to be 25.67 t/h/y and it is found in subbasin 21. Subbasin 4 has the lowest sediment yield erosion rate of 0.06 t/h/y. The total annual sediment yield in the Ketar River watershed was found to be 3784.14 t/y. The Ketar subbasins and their soil erosion rates are shown in Table 7.

The sediment yield spatial variability map of the watershed was obtained using the annual sediment yield rate from each subbasin based on erosion severity classes. The spatial distribution of sediment revealed that, out of the total 21 subbasins, six (21, 19, 15, 20, 2, and 8) had annual sediment loss rates greater than 16 tons/ha/yr. Most of them are found in the upstream and southern parts of the watershed (Figure 9). Subbasin 2 is found in the southeast of the watershed. A moderate soil erosion rate is found in the central parts of the watershed. Soil erosion rate needs to be identified at the subbasin level because it is difficult to recover once the degradation has occurred. Subbasins with a very high soil erosion rate, on the other hand, should be prioritized over subbasins with a high or moderate soil erosion rate in the land management protection system. Figure 9 shows sediment erosion-prone areas.

3.4. Rainfall, Surface Runoff, and Sediment Yield in Hotspot Subbasin. Soil erosion is mostly caused by rainfall. Rainfall has a direct impact on soil particle separation, soil aggregate degradation, and eroded sediment migration. Soil erosion generated by erosive rains accounts for the majority of total erosion. Surface runoff occurs when rainfall intensity exceeds the soil's infiltration capacity. As runoff water flows down a hill, its velocity rises, increasing the risk of erosion. Because the carried particles scrape and dislodge more soil particles, the volume of sediment increases as well. The annual average rainfall in subbasins 21, 19, and 20 is the same as the simulation, but surface runoff and sediment yield differ. This demonstrates that the amount of sediment yield in a subbasin is determined by factors other than surface runoff. Soil type, land use, land cover, and slope all play a role in determining the amount of sediment yield. Table 8 illustrates rainfall, surface runoff, and sediment yield in the hotspot area.

3.5. Land Use and Sediment Yield Relationship in Hotspot Subbasin. As indicated in Table 9, the soil erosion in critical subwatersheds is dominantly covered with cultivated land. Cultivated land can easily be eroded by runoff, wearing out the topsoil at a faster rate. A total of 1872.12 t/y of sediment was loaded from cultivated land each year, with 171.45 t/y from moderately cultivated grassland. The area covered by woodland and forested land has a lower rate of soil erosion. These six subbasins contributed 2173.71 t/y to the total annual sediment yield (3784.14 t/y).

Table 7: Ketar subbasins and their soil erosion rates.

Average annual soil erosion rate	Severity class	Subbasin number	Total area	Area cover %
0–4	Slight	18, 17, 1, 5, 4	344.41	10.24
4–8	Moderate	3, 16	195.39	5.81
8–16	High	7, 10, 6, 14, 9, 13, 11, 12	1499.52	44.60
16–32	Very high	21, 19, 15, 20, 2, 8	1322.65	39.34

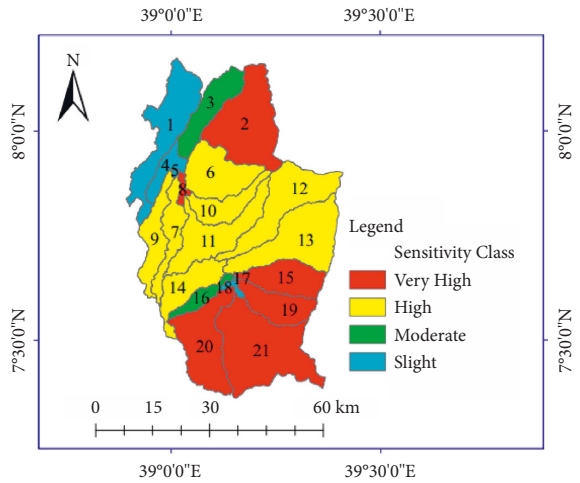

Figure 9: Sediment erosion-prone areas.

Table 8: Rainfall, surface runoff and sediment yield in the hot spot area.

Subbasin	Precipitation (mm)	Surface runoff (mm)	Sediment yield (t/y/h)	Area (km^2)
21	986.67	220.792	25.67	420.46
19	986.67	192.54	21.27	136.43
15	986.67	196.362	21.2	156.17
20	857.7	150.662	18.24	252.08
2	725.3	99.5097	17.71	341.53
8	674.75	106.199	16.45	15.97
Sum	5217.76	966.065	120.54	1322.64

Table 9: Sediment yield and land use.

Subbasin	Cultivation	Grassland (moderately cultivated)	Alpine vegetation	Open woodland	Total
2	438.27	0.11	0.23		438.61
8	210.64	1.09			211.73
15	269.24	69.47	22.42		361.13
19	283.95	27.50	16.76		328.21
20	240.83	1.47	0.17	28.17	270.64
21	429.19	71.81	62.39		563.39
Total	1872.12	171.45	101.97	28.17	2173.71

3.6. Soil Type and Sediment Yield Relationship in Hotspot Subbasin. A large amount of sediment is collected from Eutric Nitisols (1173.59 t/y), which accounts for 53.99% of the total high eroded sediment yield subbasins. About 21.27% of soil erosion was from Chromic Luvisols. The sediment yield from Haplic Xerosols is very small. Table 10 explains the soil type and sediment yield.

3.7. Slope and Sediment Yield Relationship in Hotspot Subbasin. The slope is the key determinant of soil erosion and sediment yield. As shown in Table 11, the steep slope (>35%) covers a small area, but it has a high sediment yield contribution. Areas with a slight slope (0 to 3%) contribute to a small amount of soil erosion while covering a large area. For example, in subbasin 2, a sloping rise between 3 and 12%

Table 10: Soil type and sediment yield.

Subbasin	Eutric Cambisols	Vertic Cambisols	Eutric Nitisols	Chromic Luvisols	Mollic Andosols	Pellic Vertisols	Haplic Xerosols	SDY (t/y)
2	123.07	27.37	101.87	63.86	110.38	0.1	11.96	438.61
8			134.5		76.95		0.28	211.73
15			255.93	69		36.2		361.13
19			214.21	66.17		47.83		328.21
20			135.55	135.09				270.64
21			331.53	128.28		103.58		563.39
Total	123.07	27.37	1173.59	462.4	187.33	187.71	12.24	2173.71
%	5.66	1.26	53.99	21.27	8.62	8.64	0.56	100

Table 11: Sediment yield relationship with slope and elevation in hotspot subbasin.

Subbasin	Slope	Area (km^2)	SDY (t/y)	Total SDY (t/y)	Average elevation (m)	Length (km)
2	0 to 3	43.61	5.81	438.61	2305	12.82
	12 to 20	61.78	70.16			
	20 to 35	48.7	101.18			
	3 to 12	169.61	96.49			
	>35	17.9	164.97			
8	0 to 3	1.86	2.6	211.73	2170	7.32
	12 to 20	2.33	18.42			
	20 to 35	1.56	34.44			
	3 to 12	8.36	40.4			
	>35	1.85	115.87			
15	0 to 3	12.89	12.87	361.13	2738	3.33
	12 to 20	31.93	73.53			
	20 to 35	22.31	135.01			
	3 to 12	82.17	129.34			
	>35	6.77	10.38			
19	0 to 3	12.29	11.6	328.21	2734	4.62
	12 to 20	29.35	70.81			
	20 to 35	16.55	100.95			
	3 to 12	73.9	140.66			
	>35	4.36	4.19			
20	0 to 3	22.79	5.18	270.64	2756	16.42
	12 to 20	46.41	39.05			
	20 to 35	46.34	73.26			
	3 to 12	112.03	85.28			
	>35	24.5	67.87			
21	0 to 3	35.62	12.67	563.39	2726	21.95
	12 to 20	90.96	91.91			
	20 to 35	63.84	163.67			
	3 to 12	214.31	175.54			
	>35	16.08	119.6			

has a coverage area of 169.61 km^2 and a total sediment yield of about 96.49 t/y; a slope with a percentage of rise >35% has a coverage area of only 16.9 km^2 and a total sediment yield of about 164.97 t/y. The subbasin with the highest rate of soil erosion also has the highest average elevation. The area of the watershed and the length of the channel have a strong relationship with sediment yield (Table 11). These sediments yield prone classes among all subwatersheds, requiring immediate intervention to minimize soil losses from the watershed as a whole.

4. Conclusion

Soil erosion causes the removal of top fertile soil and has a high impact on sediment yield reduction. It may also cause land degradation. The main causes of soil erosion problems today are an increase in the population, poor land-use planning, and overdependency on agriculture. Soil erosion is a critical issue in hotspot subbasins that must be addressed. The physically based, spatially distributed, and public domain SWAT model was used successfully to simulate sediment yield in the Ketar River watershed. The results of the model indicate that sediment loss rates were particularly very high in subbasins 21, 19, 20, 15, 8, and 2. The sediment yield-prone area was highly covered by cultivated land use with Eutric Nitisols. These subbasins were found on steep slopes to very steep slope intervals. Annually, about 3784.14 t/y of sediment yield was transported from the watershed and deposited at a lake located downstream of the

subbasin. Areas prone to sediment yield accounted for approximately 39.64% of total sediment yield. Sediment yield-prone areas require immediate mitigation measures from governmental and nongovernmental organizations involved in land use and land cover management.

Data Availability

All data are included in the article, and if needed, they will be submitted upon request.

Additional Points

SWAT is effectively used in modeling and simulating sediment yield. The slope of the land is the main cause of soil erosion. Steep slope with moderately cultivated land use has higher soil erosion than flat slop with highly cultivated land. Woodland and forest land even covered with steep slopes have less soil erosion rate.

Conflicts of Interest

The authors declare that they have no conflicts of interest.

References

[1] R. Hamad, K. Kolo, and H. Balzter, "Land cover changes induced by demining operations in Halgurd-Sakran national park in the Kurdistan region of Iraq," *Sustainability*, vol. 10, no. 7, pp. 2422–2515, 2018.

[2] M. C. Ramos, I. Lizaga, L. Gaspar, L. Quijano, and A. Navas, "Effects of rainfall intensity and slope on sediment, nitrogen and phosphorous losses in soils with different use and soil hydrological properties," *Agricultural Water Management*, vol. 226, Article ID 105789, 2019.

[3] J. Poesen, D. B. Torri, and T. Vanwalleghem, "Gully erosion: procedures to adopt when modelling soil erosion in landscapes affected by gullying," *Handbook of Erosion Modelling*, pp. 360–386, Academia, San Francisco, California, 2011.

[4] Y. Li, X. Lu, R. A. Washington-Allen, and Y. Li, "Micro-topographic controls on erosion and deposition of a rilled hillslope in eastern Tennessee, USA," *Remote Sensing*, vol. 14, no. 6, p. 1315, 2022.

[5] D. Pimentel, "Soil erosion: a food and environmental threat," *Environment, Development and Sustainability*, vol. 8, no. 1, pp. 119–137, 2006.

[6] R. Lal, "Soil degradation by erosion," *Land Degradation & Development*, vol. 12, no. 6, pp. 519–539, 2001.

[7] W. B. Meyer and B. L. Turner, "Human population growth and global land-use/cover change," *Annual Review of Ecology and Systematics*, vol. 23, no. 1, pp. 39–61, 1992.

[8] H. Desta and B. Lemma, "SWAT based hydrological assessment and characterization of Lake Ziway sub-watersheds, Ethiopia," *Journal of Hydrology: Regional Studies*, vol. 13, pp. 122–137, 2017.

[9] C. H. Sime, T. A. Demissie, and F. G. Tufa, "Surface runoff modeling in Ketar watershed, Ethiopia," *Journal of Sedimentary Environments*, vol. 5, Article ID 0123456789, 2020.

[10] J. G. Arnold, R. Srinivasan, R. S. Muttiah, and J. R. Williams, "Large area hydrologic modeling and assessment Part 1: model development," *Journal of the American Water Resources Association*, vol. 34, no. 1, pp. 73–89, 1998.

[11] A. Prabhanjan, E. P. Rao, and T. I. Eldho, "Application of SWAT model and geospatial techniques for sediment-yield modeling in ungauged watersheds," *Journal of Hydrologic Engineering*, vol. 20, pp. 1–6, 2015.

[12] S. Dutta and D. Sen, "Sediment distribution and its impacts on Hirakud Reservoir (India) storage capacity," *Lakes & Reservoirs: Science, Policy and Management for Sustainable Use*, vol. 21, no. 3, pp. 245–263, 2016.

[13] T. Kefay, T. Abdisa, and B. Chelkeba Tumsa, "Prioritization of susceptible watershed to sediment yield and evaluation of best management practice: a case study of awata river, southern Ethiopia," *Applied and Environmental Soil Science*, vol. 2022, Article ID 1460945, 2022.

[14] L. B. Asmamaw and A. A. Mohammed, "Identification of soil erosion hotspot areas for sustainable land management in the Gerado catchment, North-eastern Ethiopia," *Remote Sensing Applications: Society and Environment*, vol. 13, pp. 306–317, 2019.

[15] T. Getnet and A. Mulu, "Assessment of soil erosion rate and hotspot areas using RUSLE and multi-criteria evaluation technique at Jedeb watershed, Upper Blue Nile, Amhara Region, Ethiopia," *Environmental Challenges*, vol. 4, Article ID 100174, 2021.

[16] D. A. Mhiret, D. C. Dagnew, T. T. Assefa, S. A. Tilahun, B. F. Zaitchik, and T. S. Steenhuis, "Erosion hotspot identification in the sub-humid Ethiopian highlands," *Ecohydrology and Hydrobiology*, vol. 19, no. 1, pp. 146–154, 2019.

[17] S. Babar and H. Ramesh, "Streamflow response to land use land cover change over the Nethravathi river basin, India," *Journal of Hydrologic Engineering*, vol. 20, no. 10, pp. 1–11, 2015.

[18] E. Elias, "Characteristics of Nitisol profiles as affected by land use type and slope class in some Ethiopian highlands," *Environmental Systems Research*, vol. 6, no. 1, pp. 20–15, 2017.

[19] G. Fischer, F. Nachtergaele, S. Prieler, H. T. van Velthuizen, L. Verelst, and D. Wiberg, *Global Agro-Ecological Zones Assessment for Agriculture (GAEZ 2008)*, FAO, Rome, Italy, 2008.

[20] T. Li, S. Wang, B. Fu, and X. Feng, "Frequency analyses of peak discharge and suspended sediment concentration in the United States," *Journal of Soils and Sediments*, vol. 20, no. 2, pp. 1157–1168, 2020.

[21] P. M. Ndomba, F. W. Mtalo, and A. Killingtveit, "Developing an excellent sediment rating curve from one hydrological year sampling programme data: Approach," *Journal of Urban and Environmental Engineering*, vol. 2, no. 1, pp. 21–27, 2008.

[22] G. D. Glysson, *Sediment-Transport Curves*, USGS, Reston, VA, USA, 1987.

[23] T. W. Arnold, "Uninformative parameters and model selection using akaike's information criterion," *Journal of Wildlife Management*, vol. 74, no. 6, pp. 1175–1178, 2010.

[24] S. L. Neitsch, J. G. Arnold, J. R. Kiniry, and J. R. Williams, "Soil and water assessment tool theoretical documentation version 2009," 2011, https://swat.tamu.edu/media/99192/swat20.

[25] M. Geza and J. E. McCray, "Effects of soil data resolution on SWAT model stream flow and water quality predictions," *Journal of Environmental Management*, vol. 88, no. 3, pp. 393–406, 2008.

[26] Y. Her, J. Frankenberger, I. Chaubey, and R. Srinivasan, "Threshold effects in HRU definition of the soil and water assessment tool," *Transactions of the ASABE*, vol. 58, no. 2, pp. 367–378, 2015.

[27] P. J. Starks and D. N. Moriasi, "Spatial resolution effect of precipitation data on swat calibration and performance: IMPLICATIONS for ceap," *Transactions of the ASABE*, vol. 52, no. 4, pp. 1171–1180, 2009.

[28] K. C. Abbaspour, E. Rouholahnejad, S. Vaghefi, R. Srinivasan, H. Yang, and B. Kløve, "A continental-scale hydrology and water quality model for Europe: calibration and uncertainty of a high-resolution large-scale SWAT model," *Journal of Hydrology*, vol. 524, pp. 733–752, 2015.

[29] K. C. Abbaspour, C. A. Johnson, and M. T. van Genuchten, "Estimating uncertain flow and transport parameters using a sequential uncertainty fitting procedure," *Vadose Zone Journal*, vol. 3, no. 4, pp. 1340–1352, 2004.

[30] C. Zheng, M. C. Hill, G. Cao, and R. Ma, "MT3DMS: model use, calibration, and validation," *Transactions of the ASABE*, vol. 55, no. 4, pp. 1549–1559, 2012.

[31] J. C. Refsgaard, "Parameterisation, calibration and validation of distributed hydrological models," *Journal of Hydrology*, vol. 198, no. 1–4, pp. 69–97, 1997.

[32] I. Masih, S. Maskey, S. Uhlenbrook, and V. Smakhtin, "Assessing the impact of areal precipitation input on streamflow simulations using the SWAT Model1," *JAWRA Journal of the American Water Resources Association*, vol. 47, no. 1, pp. 179–195, 2011.

[33] D. N. Moriasi, M. W. Gitau, N. Pai, and P. Daggupati, "Hydrologic and water quality models: performance measures and evaluation criteria," *Transactions of the ASABE*, vol. 58, no. 6, pp. 1763–1785, 2015.

[34] T. Gashaw, T. Tulu, and M. Argaw, "Erosion risk assessment for prioritization of conservation measures in Geleda watershed, Blue Nile basin," *Ethiopia', Environmental Systems Research*, vol. 6, no. 1, pp. 1–14, 2018.

[35] R. Singh and V. S. Phadke, "Assessing soil loss by water erosion in Jamni River Basin, Bundelkhand region, India, adopting universal soil loss equation using GIS," *Current Science*, vol. 90, no. 10, pp. 1431–1435, 2006.

[36] A. Sisay, "Landscape scale soil erosion modeling and risk mapping of mountainous areas in eastern escarpment of wondo Genet watershed, Ethiopia," *International Research Journal of Arts and Social Sciences*, vol. 4, no. 6, pp. 107–116, 2014.

[37] V. Anand and B. Oinam, "Future projection and assessment of soil erosion and deposition by water in Manipur River basin using USPED model," *Geocarto International*, pp. 1–18, 2022.

[38] K. Gudeta, M. Argaw, and M. Kindu, "Identifying priority areas for conservation in mojo River watershed of Ethiopia using GIS-based erosion risk evaluation," in *State of the Art in Ethiopian Church Forests and Restoration Options*, pp. 267–285, Springer, Berlin, Germany, 2022.

[39] A. Y. Yesuph and A. B. Dagnew, "Soil erosion mapping and severity analysis based on RUSLE model and local perception in the Beshillo Catchment of the Blue Nile Basin, Ethiopia," *Environmental Systems Research*, vol. 8, no. 1, pp. 17–21, 2019.